
Exploring the Versatility of Zero-Shot CLIP for Interstitial Lung Disease Classification

Cara Van Uden^{1,2} Christian Bluethgen² Maayane Attias^{2,3} Malgorzata Polacin⁴ Haiwei Henry Guo⁵
Neha Simha⁶ Rishi Raj⁶ Curtis Langlotz²

Abstract

Interstitial lung diseases (ILD) present diagnostic challenges due to their varied manifestations and overlapping imaging features. To address this, we propose a machine learning approach that utilizes CLIP, a multimodal (image and text) self-supervised model, for ILD classification. We extensively integrate zero-shot CLIP throughout our workflow, starting from the initial extraction of image patches from volumetric CT scans and proceeding to ILD classification using "patch montages". Furthermore, we investigate how domain adaptive pretraining (DAPT) CLIP with task-specific images (CT "patch montages" extracted with ILD-specific prompts for CLIP) and/or text (lung-specific sections of radiology reports) affects downstream ILD classification performance. By leveraging CLIP-extracted "patch montages" and DAPT, we achieve strong zero-shot ILD classification results, including an AUROC of 0.893, without the need for any labeled training data. This work highlights the versatility and potential of multimodal models like CLIP for medical image classification tasks where labeled data is scarce.

1. Introduction

Interstitial lung diseases (ILD) form a diverse group of disorders that involve inflammation and fibrosis of the pul-

¹Department of Computer Science, Stanford University, Stanford, CA, USA ²Center for Artificial Intelligence in Medicine and Imaging, Stanford University, Stanford, CA, USA ³Institute for Computational and Mathematical Engineering, Stanford University, Stanford, CA, USA ⁴Stanford University, Stanford, CA, USA ⁵Department of Radiology, Stanford University School of Medicine, Stanford, CA, USA ⁶Division of Pulmonary, Allergy and Critical Care Medicine, Stanford University School of Medicine, Stanford, CA, USA. Correspondence to: Cara Van Uden <cvanuden@stanford.edu>.

Preliminary work. Under review by the International Conference on Machine Learning (ICML). Do not distribute.

monary tissue and that necessitate a consensus of radiologic, pathological, and clinical findings to establish an accurate diagnosis. Proper management of ILD requires comprehensive monitoring through CT scans and lung function tests to evaluate the evolution of the disease along with the effectiveness of treatment. As ILD encompasses a wide range of lung diseases with different etiologies and treatments, but often similar, overlapping imaging appearances, it can be challenging for clinicians to accurately identify disease progression and distinguish it from other causes of respiratory symptoms. There is currently no standardized approach for evaluating the disease progression in ILD patients, which can result in inconsistency of the interpretation of clinical data. This leads to a high inter-reader variability even among specialized radiologists and complicates the creation of sufficiently labeled datasets.

To address these challenges, we propose a novel approach that leverages multimodal deep learning techniques, specifically focusing on the combination of lung CT scans and radiology reports, to improve ILD detection and classification. Our methodology harnesses CLIP (Contrastive Language-Image Pretraining), a multimodal self-supervised learning framework that has demonstrated remarkable capabilities in capturing rich semantic representations across different modalities.

The main contributions of our work can be summarized as follows:

1. Task-specific patch retrieval: We perform zero-shot cross-modal retrieval by prompting CLIP to retrieve regions of interest ("patches") that are most likely to contain ILD-related abnormalities from each lung CT volume. This approach does not require any labeled examples or explicit annotations for ILD and demonstrates promising initial zero-shot classification performance.
2. Task-specific domain-adaptive pretraining (DAPT): We explore a domain-adaptive pretraining (DAPT) strategy that fine-tunes the CLIP model using task-specific images (CLIP-extracted "patch montages" from CT) and text (lung-specific sections of the radiology report)

and hypothesize that this may allow the model to adapt even further to the ILD domain.

3. Zero-shot ILD classification: We demonstrate strong zero-shot ILD classification performance by leveraging task-specific patch extraction and the multimodal representations learned through DAPT. Our best model achieves a zero-shot ILD classification AUROC of 0.893 without requiring any labeled examples during training. This capability significantly reduces the annotation burden, enabling effective ILD diagnosis even in scenarios where labeled data is scarce.

By combining these components, our approach achieves strong performance in ILD detection and classification while leveraging a limited number of labeled examples.

2. Related Work

Machine learning approaches have been explored for interstitial lung disease (ILD) diagnosis, addressing various aspects such as pattern detection, quantification, and prognosis. Previous studies have focused on classifying ILD cases based on standard criteria, distinguishing between different ILD subtypes, and assessing disease progression. (Barnes et al., 2022; Dack et al., 2023) highlighted the importance of multimodal and longitudinal data for diagnostic and prognostic models for ILD. (Soffer et al., 2022) highlighted the inter- and intra-observer variability and limited labeled data common in applications of machine learning to ILD. (Pawar & Talbar, 2022) present a two-stage hybrid approach for ILD classification using high-resolution computed tomography (HRCT) images, achieving accurate lung segmentation and classification into six ILD classes directly from HRCT, without the need for manual identification of the region of interest. In DeepILD (Wang et al., 2019), the authors combined semi-supervised K-means clustering and convolutional neural networks (CNNs) to perform ILD classification from CT images and achieved high performance across three chronic fibrosing ILD types. By integrating chest CT scans and clinical information, (Mei et al., 2023) leveraged multiple models to diagnose five types of ILD with multimodal data and determine a patient’s 3-year survival rate. Additionally, MIXTURE (Uegami et al., 2022) leveraged deep learning models to extract pathologically significant findings in ILD based on expert pathologists’ perspectives. These studies demonstrate the potential of machine learning in ILD diagnosis and prognosis.

Multimodal models that integrate image and text modalities have shown significant advancements in medical imaging and text analysis. CLIP leverages large-scale pretraining on natural image-text pairs to learn powerful representations for tasks like zero-shot classification, cross-modal retrieval, and visual question answering (VQA) (Radford et al.,

2021). ConVIRT (Zhang et al., 2022), GLoRIA (Huang et al., 2021), and CheXzero (Tiu et al., 2022), apply similar approaches to CLIP for the medical domain, focusing on chest X-ray interpretation with datasets like MIMIC-CXR (Johnson et al., 2019) or CheXpert (Irvin et al., 2019). CheXzero specifically enables zero-shot multi-label classification without explicit manual annotations, achieving performance comparable to expert radiologists and surpassing previous label-efficient methods. Similarly, BioMedCLIP (Zhang et al., 2023), pretrained on figure-caption pairs from biomedical research articles, achieves state-of-the-art results in various vision-language processing tasks. These multimodal models exemplify the potential of deep learning in medical imaging and text analysis, enabling improved performance and reducing the reliance on labor-intensive labeling efforts.

Our work addresses specific gaps in the current literature and is motivated by three key factors. Firstly, while previous multimodal research has primarily focused on 2D image data, such as chest X-rays, our study emphasizes the application of image/text approaches to volumetric (3D) CT data. Moreover, we specifically emphasize the utilization of fine-grained details in both image and text domains, using CT “patches” for images and lung-specific sections of text. Finally, our approach incorporates multimodal zero-shot methods at various stages of our experiment workflow, starting from the extraction of image patches from CT scans and progressing to classification, at the CT scan level, for ILD. By addressing these gaps, our work aims to enhance the understanding and classification of ILD in the context of multimodal analysis.

3. Methods

3.1. Dataset

After obtaining IRB approval, a dataset of 2303 CT studies from 1321 patients was retrieved from the hospital’s picture archiving and communication system (PACS). The cases were selected by querying the hospital’s database for patients that had received at least one CT exam following a high-resolution CT (HRCT) scan protocol for the evaluation of ILD between. The corresponding text reports of all CT scans were manually reviewed by a board-certified radiologist to assess if findings indicative of ILD had been described. A primary diagnosis likely responsible for the lung appearance was determined by a review of radiology reports and clinical notes, following multi-disciplinary team (MDT) discussion notes if available. See Table 1 for a summary of the data.

Note that we create separate labeled validation (D_{Val}) and test sets (D_{Test}), even though we do not use any labeled data during model domain-adaptive pretraining (DAPT).

	D_{All}	D_{Val}	D_{Test}
Patients (n)	1321	100	98
CT Scans (n)	2303	100	98
Age (y)	63.8	62.8	64.4
Female (%)	57.5	52.0	58.2
ILD in CT (%)	86.4	50.0	51.0
Diagnosis (%)			
IPF	14.6	27.0	16.3
SSc	10.8	16.0	22.4
HP	11.3	12.0	17.3
Other	63.3	45.0	56.1

Table 1. Dataset statistics. CT: Computed tomography. HP: Hypersensitivity pneumonitis. ILD: Interstitial lung disease. IPF: Idiopathic pulmonary fibrosis. SSc: Systemic sclerosis.

D_{Val} and D_{Test} were created by randomly sampling a total of 100 and 100 patients from D_{All} , ensuring that half of them showed signs of ILD on CT. Two patients were removed from D_{Test} after sampling because they had received lung transplants before the respective CT scan date. Before performing DAPT on D_{All} , we removed the test set from it. Therefore, the test set is disjoint from the pretrain and validation sets.

We use D_{Val} to choose our initial patch montage configuration and CLIP model for DAPT, and we evaluate our final classification models after DAPT on D_{Test} .

3.2. Data preprocessing

We perform additional preprocessing on both the image (CT volume) and text (radiology report) data. See Figure 1 for examples.

1. Image: We use only high-resolution CT (HRCT) scans. All HRCT scans were preprocessed to segment the lung tissue from the rest of the scan volume, using a combination of thresholding (-400 HU) and conventional erosion, opening and closing operations. From the segmented slices, we either extract image patches randomly or follow the patch-level classification process described in Section 3.5. We then combine the image patches into a "patch montage" image. We explore patch montage sizes of 4×4 , 8×8 , and 16×16 . We also explore a "filter threshold", in which we enforce a minimum fraction of segmented lung included in the candidate image patch. We explore "filter thresholds" of 0.2, 0.5, and 0.8.
2. Text: We extract either the impression (summary) section of the report or the lung-specific sections of the report. The lung-specific sections are those under the sub-headers "lung parenchyma", "airways", and "pleura"

in the radiology report.

3.3. Multimodal pretrained models

We investigate three multimodal pretrained models:

1. CLIP (Radford et al., 2021): CLIP is a multimodal image-text model. This specific pretrained CLIP model uses a Vision Transformer (ViT) for its image encoder, and a Transformer as its text encoder. It was pretrained on the LAION-2B English subset of the LAION-5B dataset (Schuhmann et al., 2022). We explore two different CLIP models with different ViT-B image encoders—ViT-B/16 and ViT-B/32.
2. BioMed-CLIP (Zhang et al., 2023): BioMed-CLIP is a CLIP-style model pretrained on PMC-15M, a dataset of 15 million figure-caption pairs from biomedical research articles in PubMed Central. It consists of a PubMedBERT (Gu et al., 2020) text encoder and a Vision Transformer image encoder. With domain-specific adaptations, it excels in vision-language processing tasks like cross-modal retrieval, image classification, and visual question answering in the biomedical domain.
3. CheXzero (Tiu et al., 2022): CheXzero is a CLIP-style model initialized with pretrained weights from OpenAI’s CLIP model. It utilizes the same ViT-B/32 architecture as our pretrained CLIP model. It is trained on the MIMIC-CXR dataset and uses the impressions section of each text report in its (image, text) pretraining pair. CheXzero demonstrates the ability to train a zero-shot model for domain-specific medical tasks.

3.4. Domain-adaptive pretraining

We perform domain-adaptive pretraining (DAPT) (Gururangan et al., 2020) to adapt CLIP model to the ILD domain. We initialize from the CLIP model configuration that achieved the best zero-shot image-level ILD classification on the validation set. We then perform further contrastive pretraining using pairs of extracted "patch montages" (either random or CLIP-retrieved) and radiology report text (either impression or lung-specific sections). We train for up to 10 epochs with early stopping (patience of 1,000 steps) and save a model checkpoint every 100 steps. We perform a hyperparameter search over learning rate for five values in the range $[1e^{-5}, \dots, 1e^{-3}]$. We hold out 10% of the DAPT pretraining set as a validation set and choose the best model checkpoint as that which achieved the lowest validation set loss.

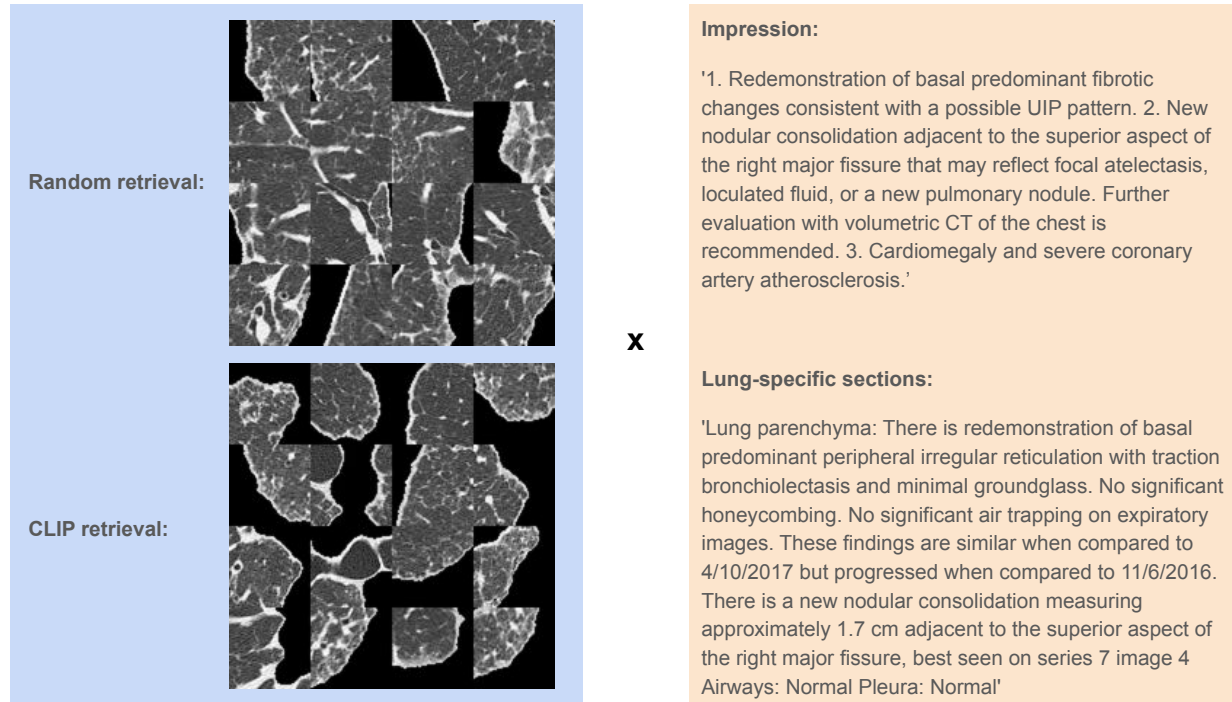


Figure 1. Example of 4×4 patch montage image and accompanying radiology report text. Patch montage images can be created with randomly-retrieved patches or with CLIP-retrieved patches, and text can be extracted from the impression or lung-specific sections.

3.5. Zero-shot classification

To assess the model’s zero-shot performance in patch and patch montage classification, we utilized a positive–negative softmax evaluation method for each disease, following the procedure in CheXzero (Tiu et al., 2022). Here’s how the procedure works: First, we calculate logits using positive prompts (e.g., “interstitial lung disease”) and negative prompts (“no interstitial lung disease”). Then, we compute the softmax between the positive and negative logits. Finally, we consider the softmax probabilities of the positive logits as the likelihood of the disease being present in the CT image patch.

We perform two stages of zero-shot classification:

1. Patch-level classification: We use this to rank the most task-specific (ILD-specific) patches from each CT volume when constructing “patch montages”. The most ILD-specific patches are those with the highest softmax probability of “interstitial lung disease” over “no interstitial lung disease”.
2. Volume- (“patch montage-”) level classification: We use this to classify the “patch montage” extracted from each CT volume as positive or negative for ILD or one of its subtypes. The probability of disease is calculated as the softmax probability of “{disease name}” over “no {disease name}”.

3.6. Reader study

We qualitatively evaluate our results via a reader study, in which we aim to compare randomly-retrieved, CLIP-retrieved, and DAPT-CLIP retrieved patch montages. We ask two board-certified radiologists to label and count the number of ILD-specific patches in each “patch montage” after patch extraction.

4. Experiments

Please see Figure 2 for an overview of our experiments. We perform the following experiments:

1. Initial zero-shot classification of patch montages. Patch montages are extracted randomly or extracted via zero-shot prompting of a CLIP (CLIP, CheXzero, or BioMed-CLIP) pretrained model. Best performance here determines which CLIP model and montage size we use for DAPT.
2. We perform DAPT for each combination of images (random; CLIP-retrieved extracted patch montage) and text (impression; lung section). This creates a set of four “DAPT-CLIP” models.
3. Zero-shot classification of patch montages using DAPT-CLIP models. We evaluate using a single model checkpoint and using a model ensemble.

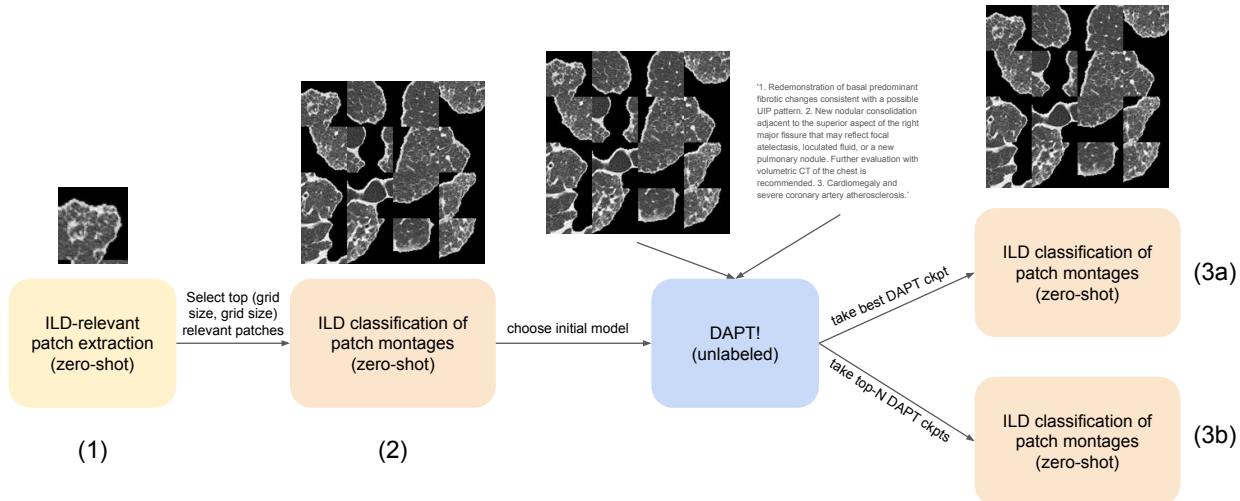


Figure 2. The experiment workflow. Note our usage of zero-shot CLIP at multiple stages of the workflow: (1) to choose our initial task-specific patches, (2) to perform initial zero-shot classification of "patch montages" and determine our model to use for DAPT, and (3a,b) to perform post-DAPT zero-shot classification using either a single model checkpoint or a model ensemble.

5. Results

5.1. Initial zero-shot classification

We find that CheXzero, with randomly-retrieved patches, a patch montage of size 16×16 , and a filter threshold of 0.5, achieves the best zero-shot ILD classification performance, achieving an AUROC of 0.771, AUPRC of 0.768, and F1-score of 0.730 on our validation set (see Table 2 for details). However, CheXzero, with either patch retrieval method, a patch montage of size 4×4 , and a filter threshold of 0.5, achieve the next-best performance. As we test random and CLIP (CheXzero)-retrieved performance further against DAPT-CLIP, we choose to use CheXzero and a 4×4 patch size moving forward. We therefore use this CheXzero 4×4 configuration to perform image preprocessing across the entire ILD dataset for later DAPT pretraining.

For CheXzero with CheXzero-retrieved patches, a 4×4 patch montage size, and a 0.5 filter threshold, we achieve an AUROC of 0.674, AUPRC of 0.652, and F1-score of 0.705 on our validation set. In contrast to the relatively higher performance on the validation set, we later achieved an AUROC of 0.584, AUPRC of 0.602, and F1-score of 0.667 on the test set using this initial zero-shot approach.

5.2. DAPT zero-shot classification

We find that a DAPT-CLIP model pretrained on (CLIP (CheXzero)-retrieved 4×4 patch montage, impression) pairs achieves best performance when paired with DAPT-CLIP patch montage extraction at test time, achieving an AUROC of 0.893, AUPRC of 0.917, and F1-score of 0.824 on our test set. This is an increase of 0.309 AUROC, 0.315

AUPRC, and 0.157 F1 over the comparable model before DAPT (see Section 5.1). Comparing our best Impressions-CLIP- 4×4 model against its random-patch-montage counterpart (Impressions-Random- 4×4), we see an increase in downstream classification performance when using CLIP to create patch montages during DAPT. In line with our hypothesis, we also see an even further increase in performance when then using the trained DAPT-CLIP model to retrieve patches at test time (Impressions-CLIP- 4×4 for patch montage retrieval + Impressions-CLIP- 4×4 for classification). Contrary to our initial hypothesis, we see a degradation in performance when using lung-related radiology report sections as text during DAPT across our DAPT-CLIP models.

We also evaluate the classification performance of an ensemble of five DAPT-CLIP models, selected as the top five best checkpoints during DAPT by validation loss, and find no significant change in performance after ensembling. See Tables 3 and 5 for details.

Finally, we evaluate zero-shot ILD *subtype* classification for three ILD subtypes: idiopathic pulmonary fibrosis (IPF), systemic sclerosis (SSc), and hypersensitivity pneumonitis (HP) with our best DAPT-CLIP model. Zero-shot classification of these subtypes is a more difficult task than general ILD classification; we achieve a zero-shot performance of 0.800 AUROC for IPF, 0.649 for SSc, and 0.639 for HP. See Table 4 for details.

5.3. Reader study

We examine the patches retrieved by our best DAPT-CLIP (see Table 3) model against random patch retrieval and CLIP patch retrieval in a set of reader studies. Please see Figure

Exploring the Versatility of Zero-Shot CLIP for Interstitial Lung Disease Classification

Patch Montage Method	Classification Model	Montage Size	AUROC	AUPRC	F1
Random	CLIP (ViT-B/16)	4 × 4	0.470	0.476	0.658
		8 × 8	0.515	0.504	0.662
		16 × 16	0.432	0.475	0.667
Random	CLIP (ViT-B/32)	4 × 4	0.537	0.518	0.662
		8 × 8	0.485	0.491	0.662
		16 × 16	0.458	0.531	0.662
Random	BioMed-CLIP (ViT-B/16)	4 × 4	0.541	0.532	0.662
		8 × 8	0.512	0.507	0.676
		16 × 16	0.580	0.669	0.667
Random	CheXzero (ViT-B/32)	4 × 4	<u>0.682</u>	<u>0.727</u>	<u>0.672</u>
		8 × 8	0.624	0.639	0.656
		16 × 16	0.771	0.768	0.730
CLIP (ViT-B/16)	CLIP (ViT-B/16)	4 × 4	0.422	0.439	0.681
		8 × 8	0.502	0.513	0.671
		16 × 16	0.419	0.442	0.658
CLIP (ViT-B/32)	CLIP (ViT-B/32)	4 × 4	0.405	0.461	0.662
		8 × 8	0.422	0.457	0.662
		16 × 16	0.440	0.511	0.658
BioMed-CLIP (ViT-B/16)	BioMed-CLIP (ViT-B/16)	4 × 4	0.617	<u>0.635</u>	<u>0.686</u>
		8 × 8	0.566	0.544	0.672
		16 × 16	0.569	0.578	0.662
CheXzero (ViT-B/32)	CheXzero (ViT-B/32)	4 × 4	0.674	0.652	0.705
		8 × 8	0.530	0.515	0.653
		16 × 16	<u>0.650</u>	0.612	0.682

Table 2. Zero-shot ILD classification performance on the validation set using patch montages. We vary the pretrained CLIP model used for patch retrieval and classification, as well as the patch montage size. We fix the filter threshold at 0.5; please see the complete results for filter thresholds 0.2 and 0.8 in Tables 7 and 8 in the Appendix. We find that CheXzero, with random patches and with a patch montage of size 16 × 16 achieves the best zero-shot ILD classification performance. However, CheXzero, with either patch type and with a patch montage of size 4 × 4 achieve the next-best performance. As we test random vs CLIP-retrieved performance further after DAPT, we choose to use CheXzero and a 4 × 4 patch size moving forward. Please see Section 5.1 for the best method’s result on the test set.

Classification Model (DAPT-CLIP)	Patch Montage Method	AUROC	AUPRC	F1
Impressions-Random-4 × 4	Random	0.797	0.824	0.744
	CLIP	0.857	0.868	0.811
	DAPT-CLIP	0.802	0.846	0.752
Sections-Random-4 × 4	Random	0.798	0.818	0.776
	CLIP	0.844	0.858	0.807
	DAPT-CLIP	0.821	0.841	0.792
Impressions-CLIP-4 × 4	Random	0.835	0.814	0.781
	CLIP	0.850	0.872	0.774
	DAPT-CLIP	0.893	0.917	0.824
Sections-CLIP-4 × 4	Random	0.770	0.797	0.674
	CLIP	0.786	0.824	0.742
	DAPT-CLIP	0.760	0.810	0.716

Table 3. Zero-shot ILD classification on the test set after domain-adaptive CLIP pretraining (DAPT-CLIP). We test each combination of DAPT-CLIP classification model and test-time patch extraction method. We find that a DAPT-CLIP model pretrained on (CLIP (CheXzero)-retrieved 4 × 4 patch montage, impression) pairs achieves best performance when paired with DAPT-CLIP patch montage extraction at test time.

3 for an example of the ILD-specific patches retrieved randomly, by the CLIP model (CheXzero) before DAPT, and

by the best CLIP model (CheXzero) after DAPT.

Based on the results of our reader study, where readers

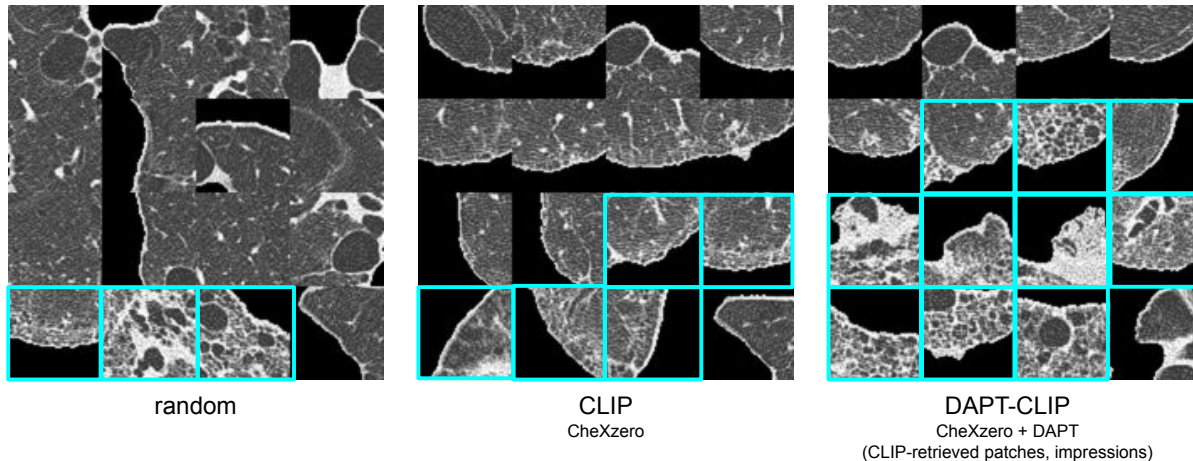


Figure 3. Examples of the patches retrieved randomly, by CLIP (CheXzero), and by DAPT-CLIP (our best CheXzero + DAPT model) for a single example CT scan. ILD-specific patches (boxed in blue) were labeled by a board-certified radiologist. For this CT scan, out of the 16 patches in the montage, random retrieves 3 relevant patches, CLIP retrieves 5, and DAPT-CLIP retrieves 10 patches.

ILD Subtype	AUROC	AUPRC	F1
IPF	0.800	0.403	0.500
SSc	0.649	0.329	0.442
HP	0.639	0.242	0.351

Table 4. Zero-shot ILD subtype classification on the test set with the best DAPT-CLIP model (Impressions-CLIP-4 × 4). The three subtypes classified here are idiopathic pulmonary fibrosis (IPF), systemic sclerosis (SSc), and hypersensitivity pneumonitis (HP).

reported the number of ILD-specific patches (see Table 6), we can draw the following conclusions:

- For the ILD-positive patients, DAPT-CLIP retrieval outperformed the two other methods. Readers counted on average 10.1 out of 16 patches (63.2%) for the DAPT-CLIP method, 7.9 out of 16 (49.4%) for the CLIP method and 5.9 out of 16 patches (37.1%) for the random method. This indicates that the DAPT-CLIP model-based method is more effective in retrieving ILD-specific patches for positive patients.
- For ILD-negative patients, all three methods show a low percentage of reported abnormal patches, which aligns with the absence of visible ILD abnormalities in their CT scans. Readers counted, on average, 1.4 out of 16 patches (9.0%) for the DAPT-CLIP method, 1.5 out of 16 (9.6%) for the CLIP method and 1.3 out of 16 patches (8.3%) for the random method. These findings indicate that the models, particularly DAPT-CLIP, detect subtle clinical abnormalities that are also identified by the readers. However, it is important to consider that these abnormalities may not have clinical significance, or there is a possibility of false positives among the reported patches.
- To verify inter-reader agreement, we computed the interclass correlation coefficient (ICC) (Bartko, 1966;

Koo & Li, 2016), a statistical measure used to quantify the level of consistency between readers. As seen in 6, DAPT-CLIP achieves the highest ICC for both ILD-positive and -negative patients across the three patch retrieval methods, and the ICC scores shows good agreement for the ILD positive (0.794) and negative patients (0.757) for DAPT-CLIP. This slight difference in ICC scores between the positive and negative patients could be attributed to the subjectivity and complexity of interpretation of ILD abnormal patches. The absence of apparent abnormalities for ILD negative patients could lead to differences in interpretation among the readers, resulting in lower agreement. On the contrary, the ILD positive group might have exhibited more consistent and visually striking abnormalities, making them easier to identify and agree upon.

6. Conclusion

In this work, we demonstrate the versatility and effectiveness of zero-shot CLIP in the classification of interstitial lung disease (ILD). By leveraging zero-shot CLIP at various stages of our experiment workflow, from extracting initial patches to "patch montage" classification, we achieve strong ILD classification results (AUROC of 0.893, AUPRC of 0.917, and F1-score of 0.824) without the need for any labeled training data. The combination of task-specific im-

Exploring the Versatility of Zero-Shot CLIP for Interstitial Lung Disease Classification

Classification Model (DAPT-CLIP)	Patch Montage Method	AUROC	AUPRC	F1
Impressions-Random-4 × 4	Random	0.806	0.812	0.783
	CLIP	0.832	0.850	0.777
	DAPT-CLIP	0.841	0.872	0.816
Sections-Random-4 × 4	Random	0.782	0.819	0.739
	CLIP	0.816	0.838	0.767
	DAPT-CLIP	0.763	0.793	0.736
Impressions-CLIP-4 × 4	Random	0.796	0.795	0.789
	CLIP	0.882	0.885	0.808
	DAPT-CLIP	0.892	0.913	0.833
Sections-CLIP-4 × 4	Random	0.783	0.829	0.739
	CLIP	0.840	0.874	0.771
	DAPT-CLIP	0.835	0.882	0.773

Table 5. Zero-shot ILD classification on the test set, using an ensemble of 5 models, after domain-adaptive CLIP pretraining (DAPT-CLIP). We test each combination of DAPT-CLIP classification model and test-time patch extraction method.

ILD	Patch Montage Method	% of Patch Montage with ILD (Average)	ICC(3,1) Score
Negative	Random	8.3%	0.656
	CLIP	9.6%	0.422
	DAPT-CLIP	9.0%	0.757
Positive	Random	37.1%	0.612
	CLIP	49.4%	0.700
	DAPT-CLIP	63.2%	0.794

Table 6. Reader study results. We compare randomly-retrieved, CLIP-retrieved, and DAPT-CLIP retrieved patch montages. Two board-certified radiologists counted the number of ILD-specific patches in each patch montage. We find that DAPT-CLIP retrieves the most ILD patches (on average) and has the highest interreader agreement.

age patch retrieval and domain-adaptive pretraining, both with CLIP, proves to be a powerful approach for ILD classification.

Moreover, our findings indicate potential avenues for further improvement and exploration. Varying the prompts used for patch retrieval can serve as a valuable data augmentation strategy when creating "patch montages," potentially improving the robustness and generalizability of our model. We also see potential in using these models for other tasks relevant for ILD, such as predicting ILD prognosis. Another promising direction is to extend the use of our approach to finer-grained patch retrieval and classification. We performed initial experiments in zero-shot ILD subtype classification; further work in this direction would improve the clinical utility of our approach and provide more targeted insights for patient care and treatment planning. By targeting specific clinical observations for patch retrieval, such as reticulation, ground-glass opacities, or honeycombing, we could potentially further improve performance of our approach for diagnosis and prognosis of ILD and its subtypes.

This work highlights the significant contributions that can be made by leveraging multimodal pretrained models like CLIP in versatile ways for medical image classification, particularly in settings with limited labeled data. We hope

that this work inspires further exploration and research in this direction.

7. Acknowledgements

This study is supported by Boehringer Ingelheim Pharmaceuticals, Inc. (BIPI) in collaboration with the Stanford Interstitial Lung Diseases program and the Stanford Center for Artificial Intelligence in Medicine and Imaging. CL is supported in part by the Medical Imaging and Data Resource Center (MIDRC), funded by the National Institute of Biomedical Imaging and Bioengineering (NIBIB) of the National Institutes of Health under contract 75N92020C00021.

References

- Barnes, H., Humphries, S. M., George, P. M., Assayag, D., Glaspole, I., Mackintosh, J. A., Corte, T. J., Glassberg, M., Johannson, K. A., Calandriello, L., et al. Machine learning in radiology: the new frontier in interstitial lung diseases. *The Lancet Digital Health*, 2022.
- Bartko, J. J. The intraclass correlation coefficient as a measure of reliability. *Psychological reports*, 19(1):3–11, 1966.
- Dack, E., Christe, A., Fontanellaz, M., Brigato, L., Heverhagen, J. T., Peters, A. A., Huber, A. T., Hoppe, H., Mougiakakou, S., and Ebner, L. Artificial intelligence and interstitial lung disease: Diagnosis and prognosis. *Investigative radiology*, pp. 10–1097, 2023.
- Gu, Y., Tinn, R., Cheng, H., Lucas, M., Usuyama, N., Liu, X., Naumann, T., Gao, J., and Poon, H. Domain-specific language model pretraining for biomedical natural language processing, 2020.
- Gururangan, S., Marasović, A., Swayamdipta, S., Lo, K., Beltagy, I., Downey, D., and Smith, N. A. Don't stop pretraining: Adapt language models to domains and tasks. *arXiv preprint arXiv:2004.10964*, 2020.
- Huang, S.-C., Shen, L., Lungren, M. P., and Yeung, S. Gloria: A multimodal global-local representation learning framework for label-efficient medical image recognition. In *Proceedings of the IEEE/CVF International Conference on Computer Vision*, pp. 3942–3951, 2021.
- Irvin, J., Rajpurkar, P., Ko, M., Yu, Y., Ciurea-Ilcus, S., Chute, C., Marklund, H., Haghgoo, B., Ball, R., Shpankaya, K., et al. Chexpert: A large chest radiograph dataset with uncertainty labels and expert comparison. In *Proceedings of the AAAI conference on artificial intelligence*, volume 33, pp. 590–597, 2019.
- Johnson, A. E., Pollard, T. J., Berkowitz, S. J., Greenbaum, N. R., Lungren, M. P., Deng, C.-y., Mark, R. G., and Horng, S. Mimic-cxr, a de-identified publicly available database of chest radiographs with free-text reports. *Scientific data*, 6(1):317, 2019.
- Koo, T. K. and Li, M. Y. A guideline of selecting and reporting intraclass correlation coefficients for reliability research. *Journal of chiropractic medicine*, 15(2):155–163, 2016.
- Mei, X., Liu, Z., Singh, A., Lange, M., Boddu, P., Gong, J. Q., Lee, J., DeMarco, C., Cao, C., Platt, S., et al. Interstitial lung disease diagnosis and prognosis using an ai system integrating longitudinal data. *Nature Communications*, 14(1):2272, 2023.
- Pawar, S. P. and Talbar, S. N. Two-stage hybrid approach of deep learning networks for interstitial lung disease classification. *BioMed Research International*, 2022, 2022.
- Radford, A., Kim, J. W., Hallacy, C., Ramesh, A., Goh, G., Agarwal, S., Sastry, G., Askell, A., Mishkin, P., Clark, J., et al. Learning transferable visual models from natural language supervision. In *International conference on machine learning*, pp. 8748–8763. PMLR, 2021.
- Schuhmann, C., Beaumont, R., Vencu, R., Gordon, C., Wightman, R., Cherti, M., Coombes, T., Katta, A., Mullis, C., Wortsman, M., et al. Laion-5b: An open large-scale dataset for training next generation image-text models. *arXiv preprint arXiv:2210.08402*, 2022.
- Soffer, S., Morgenthau, A. S., Shimon, O., Barash, Y., Konen, E., Glicksberg, B. S., and Klang, E. Artificial intelligence for interstitial lung disease analysis on chest computed tomography: a systematic review. *Academic Radiology*, 29:S226–S235, 2022.
- Tiu, E., Talius, E., Patel, P., Langlotz, C. P., Ng, A. Y., and Rajpurkar, P. Expert-level detection of pathologies from unannotated chest x-ray images via self-supervised learning. *Nature Biomedical Engineering*, pp. 1–8, 2022.
- Uegami, W., Bychkov, A., Ozasa, M., Uehara, K., Kataoka, K., Johkoh, T., Kondoh, Y., Sakanashi, H., and Fukuoka, J. Mixture of human expertise and deep learning—developing an explainable model for predicting pathological diagnosis and survival in patients with interstitial lung disease. *Modern Pathology*, 35(8):1083–1091, 2022.
- Wang, C., Moriya, T., Hayashi, Y., Roth, H., Lu, L., Oda, M., Ohkubo, H., and Mori, K. Weakly-supervised deep learning of interstitial lung disease types on ct images. In *Medical Imaging 2019: Computer-Aided Diagnosis*, volume 10950, pp. 373–379. SPIE, 2019.
- Zhang, S., Xu, Y., Usuyama, N., Bagga, J., Tinn, R., Preston, S., Rao, R., Wei, M., Valluri, N., Wong, C., et al. Large-scale domain-specific pretraining for biomedical vision-language processing. *arXiv preprint arXiv:2303.00915*, 2023.
- Zhang, Y., Jiang, H., Miura, Y., Manning, C. D., and Langlotz, C. P. Contrastive learning of medical visual representations from paired images and text. In *Machine Learning for Healthcare Conference*, pp. 2–25. PMLR, 2022.

A. Appendix

Patch Montage Method	Classification Model	Montage Size	AUROC	AUPRC	F1
Random	CLIP (ViT-B/16)	4	0.432	0.463	0.662
	CLIP (ViT-B/16)	8	0.380	0.433	0.662
	CLIP (ViT-B/16)	16	0.521	0.521	0.658
Random	CLIP (ViT-B/32)	4	0.454	0.476	0.662
	CLIP (ViT-B/32)	8	0.552	0.587	0.667
	CLIP (ViT-B/32)	16	0.472	0.524	0.667
Random	BioMed-CLIP (ViT-B/16)	4	0.498	0.530	0.662
	BioMed-CLIP (ViT-B/16)	8	0.610	0.592	0.676
	BioMed-CLIP (ViT-B/16)	16	0.598	0.656	0.658
Random	CheXzero (ViT-B/32)	4	0.581	0.636	0.671
	CheXzero (ViT-B/32)	8	0.568	0.556	0.667
	CheXzero (ViT-B/32)	16	0.598	0.602	0.658
CLIP (ViT-B/16)	CLIP (ViT-B/16)	4	0.470	0.518	0.658
	CLIP (ViT-B/16)	8	0.452	0.468	0.658
	CLIP (ViT-B/16)	16	0.423	0.436	0.662
CLIP (ViT-B/32)	CLIP (ViT-B/32)	4	0.424	0.466	0.658
	CLIP (ViT-B/32)	8	0.443	0.462	0.658
	CLIP (ViT-B/32)	16	0.485	0.535	0.658
BioMed-CLIP (ViT-B/16)	BioMed-CLIP (ViT-B/16)	4	0.551	0.607	0.658
	BioMed-CLIP (ViT-B/16)	8	0.440	0.450	0.658
	BioMed-CLIP (ViT-B/16)	16	0.601	0.633	0.676
CheXzero (ViT-B/32)	CheXzero (ViT-B/32)	4	0.671	0.708	0.640
	CheXzero (ViT-B/32)	8	0.618	0.585	0.667
	CheXzero (ViT-B/32)	16	0.653	0.635	0.692

Table 7. Zero-shot ILD classification performance on the validation set using patch montages. We vary the pretrained CLIP model used for patch retrieval and classification, as well as the patch montage size. We fix the filter threshold at 0.2.

Patch Montage Method	Classification Model	Montage Size	AUROC	AUPRC	F1
Random	CLIP (ViT-B/16)	4	0.524	0.506	0.658
	CLIP (ViT-B/16)	8	0.388	0.462	0.658
	CLIP (ViT-B/16)	16	0.556	0.576	0.667
Random	CLIP (ViT-B/32)	4	0.440	0.497	0.662
	CLIP (ViT-B/32)	8	0.459	0.478	0.658
	CLIP (ViT-B/32)	16	0.564	0.612	0.681
Random	BioMed-CLIP (ViT-B/16)	4	0.435	0.448	0.658
	BioMed-CLIP (ViT-B/16)	8	0.507	0.575	0.658
	BioMed-CLIP (ViT-B/16)	16	0.620	0.651	0.667
Random	CheXzero (ViT-B/32)	4	0.599	0.627	0.676
	CheXzero (ViT-B/32)	8	0.753	0.742	0.706
	CheXzero (ViT-B/32)	16	0.636	0.614	0.705
CLIP (ViT-B/16)	CLIP (ViT-B/16)	4	0.530	0.541	0.662
	CLIP (ViT-B/16)	8	0.558	0.581	0.662
	CLIP (ViT-B/16)	16	0.402	0.448	0.662
CLIP (ViT-B/32)	CLIP (ViT-B/32)	4	0.424	0.476	0.658
	CLIP (ViT-B/32)	8	0.494	0.505	0.671
	CLIP (ViT-B/32)	16	0.492	0.523	0.667
BioMed-CLIP (ViT-B/16)	BioMed-CLIP (ViT-B/16)	4	0.504	0.528	0.667
	BioMed-CLIP (ViT-B/16)	8	0.636	0.680	0.667
	BioMed-CLIP (ViT-B/16)	16	0.575	0.644	0.657
CheXzero (ViT-B/32)	CheXzero (ViT-B/32)	4	0.593	0.575	0.667
	CheXzero (ViT-B/32)	8	0.660	0.631	0.693
	CheXzero (ViT-B/32)	16	0.536	0.530	0.662

Table 8. Zero-shot ILD classification performance on the validation set using patch montages. We vary the pretrained CLIP model used for patch retrieval and classification, as well as the patch montage size. We fix the filter threshold at 0.8.